# Supporting Information

## Mechanistic Insights on Sulfur Functionalization of Ag Nanoflowers

Arup K. De [1,†], Ravishankar Srivastava [1,†], Nirupam Das [1], Partho Sarathi Gooh Pattader[1,2,3,*], and Rajiv K. Kar [1,2,*]

[1] Jyoti and Bhupat Mehta School of Health Sciences and Technology, Indian Institute of Technology Guwahati, Guwahati, Assam 781039, India;
[2] Centre for Nanotechnology, Indian Institute of Technology Guwahati, Guwahati, Assam 781039, India;
[3] Department of Chemical Engineering, Indian Institute of Technology Guwahati, Guwahati, Assam 781039, India

**Table of Contents**

## Details of systems simulated with classical mechanics

The computational systems were modelled based on the experimental molar ratio. In all systems, we considered 1001 Ag atoms, assuming it to be equivalent to 77 nanoclusters and 10 PVP residues, equivalent to 100 atoms. The T0 model does not contain any Tu molecules, while T0.5 and T1 models contain 100 and 200 Tu molecules, respectively. The number of EG molecules is constant at 4000 in all systems.

**Table S1. Details of all the systems with the number of atoms and residues.**

| Atoms/Molecules | Total no. of atoms | | |
|---|---|---|---|
| **Ag** | 1001 (77 *) | | |
| **EG** | 40000 (4000 **) | | |
| **PVP** | 100 (10 **) | | |
| **Tu** | 0 **(T0)** | 800 **(T0.5)**<br>(100 **) | 1600 **(T1)**<br>(200 **) |

Notes: * refers to nanoclusters; ** refers to residues

**Table S2. Simulated box dimensions of T0, T0.5, and T1 at equilibrium.**

| System | Final Simulation Box Dimension |
|---|---|
| **T0** | 38.9 x 40.9 x 39.0 |
| **T0.5** | 40.7 x 41.2 x 49.6 |
| **T1** | 62.7 x 56.8 x 41.8 |

The experimental molar ratio of Ag: PVP: Tu is 5: 0.05: 1 but for SAPT energy calculations, the molecule ratio is 7: 1: 1. Therefore, we have normalised the calculated SAPT energy per Ag atom in Table S3. We observed a similar trend of stabilization in SAPT and MD simulated energies. Tu incorporates the highest stabilisation in the Ag-PVP-Tu system in comparison with the other systems.

**Table S3. Normalised SAPT and MD simulated potential energies for various systems.**

| System | SAPT Energy per Ag atom (kcal/mole) | | | | | MD potential energy per Ag atom (kcal/mole) |
|---|---|---|---|---|---|---|
| | Electrostatic interaction | Exchange energy | Induction energy | Dispersion energy | SAPT0 | |
| Ag-PVP | -3.63 | 4.36 | -1.58 | -2.01 | -2.86 | T0 = -27.43 |
| Ag-PVP-Tu | -4.37 | 5.45 | -2.17 | -2.85 | -3.94 | T0.5 = -34.41<br>T1 = -41.35 |
| Ag-Tu | -0.73 | 1.1 | -0.61 | -0.61 | -0.86 | |

## FE-SEM study

Field Emission Scanning Electron Microscopy (FE-SEM) images were taken with the instrument magnifications of 10X to 300000X. A 1x1 cm$^2$ silicon wafer was properly washed with warm acetone for 15-20 min, then placed in methanol for 3 min, rinsed with DI water. Then the wafers were applied in freshly prepared Piranha solution to clean the organic impurities followed by thoroughly washed with DI water and dried at 50 °C. The experimented samples were dispersed in isopropanol and drop casted on the cleaned dry wafer. After that the sample was dried at 45 °C on a hot plate before put on the instrument's sample holder. Sulfur peaks are not observed in T0 sample, while in T0.5 and T1, there is a clear observation of sulfur peak. The intensity of sulfur peak get enhanced from T0.5 to T1 indicating the effect of increment of Tu concentration.

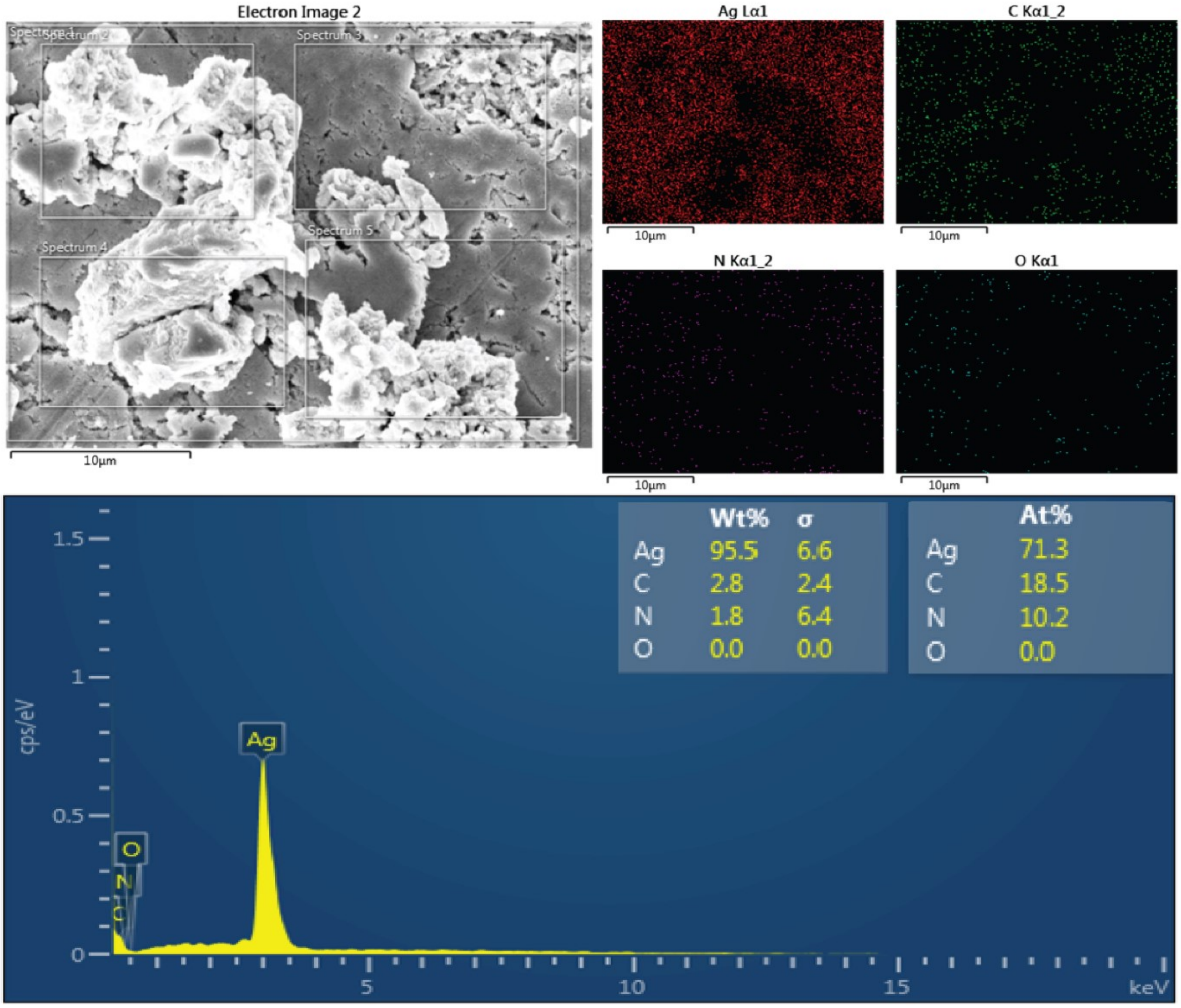

|  | Wt% | σ |
|---|---|---|
| Ag | 95.5 | 6.6 |
| C | 2.8 | 2.4 |
| N | 1.8 | 6.4 |
| O | 0.0 | 0.0 |

|  | At% |
|---|---|
| Ag | 71.3 |
| C | 18.5 |
| N | 10.2 |
| O | 0.0 |

**Figure S1. EDX analysis of T0 system.**

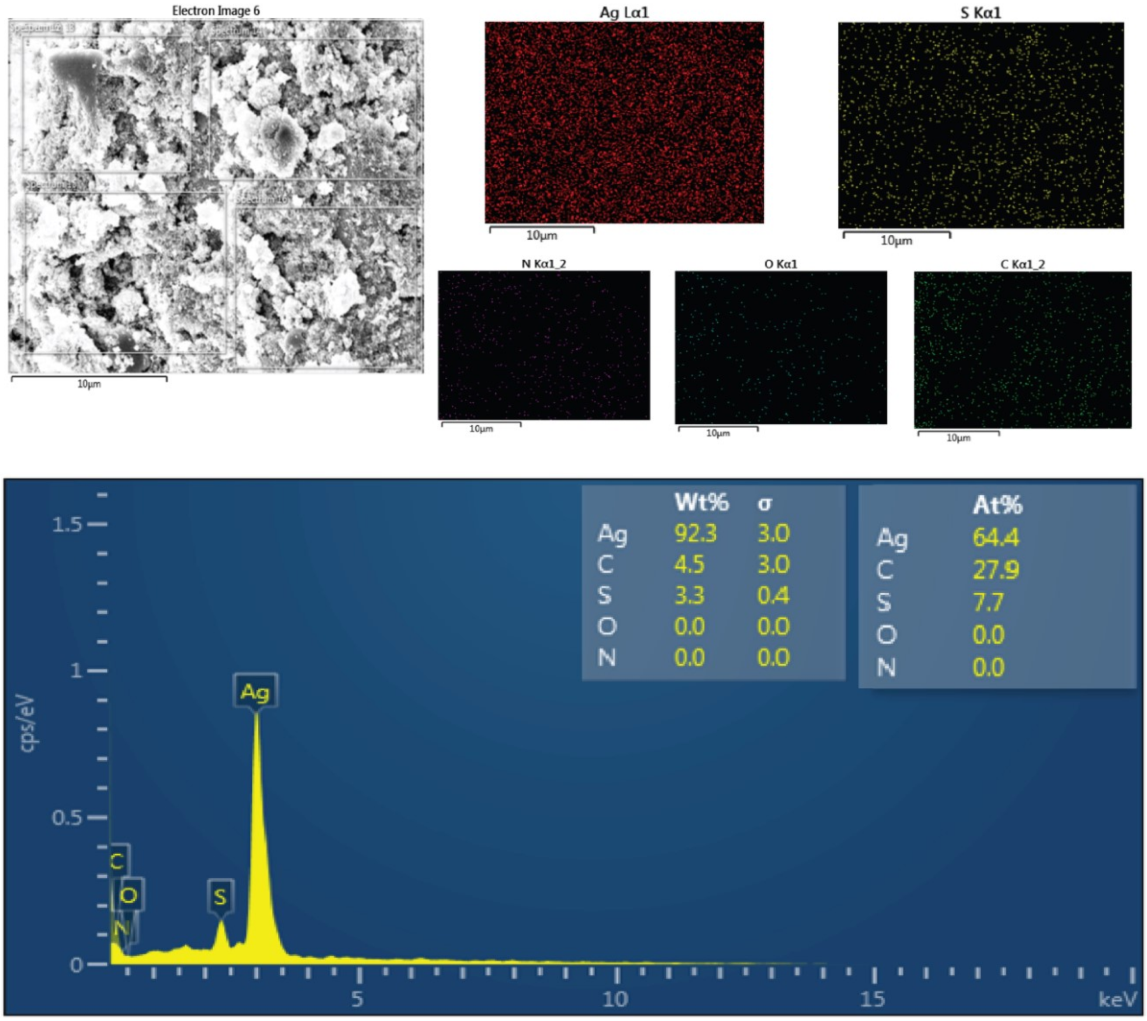

| | Wt% | σ |
|---|---|---|
| Ag | 92.3 | 3.0 |
| C | 4.5 | 3.0 |
| S | 3.3 | 0.4 |
| O | 0.0 | 0.0 |
| N | 0.0 | 0.0 |

| | At% |
|---|---|
| Ag | 64.4 |
| C | 27.9 |
| S | 7.7 |
| O | 0.0 |
| N | 0.0 |

**Figure S2. EDX analysis of T0.5 system.**

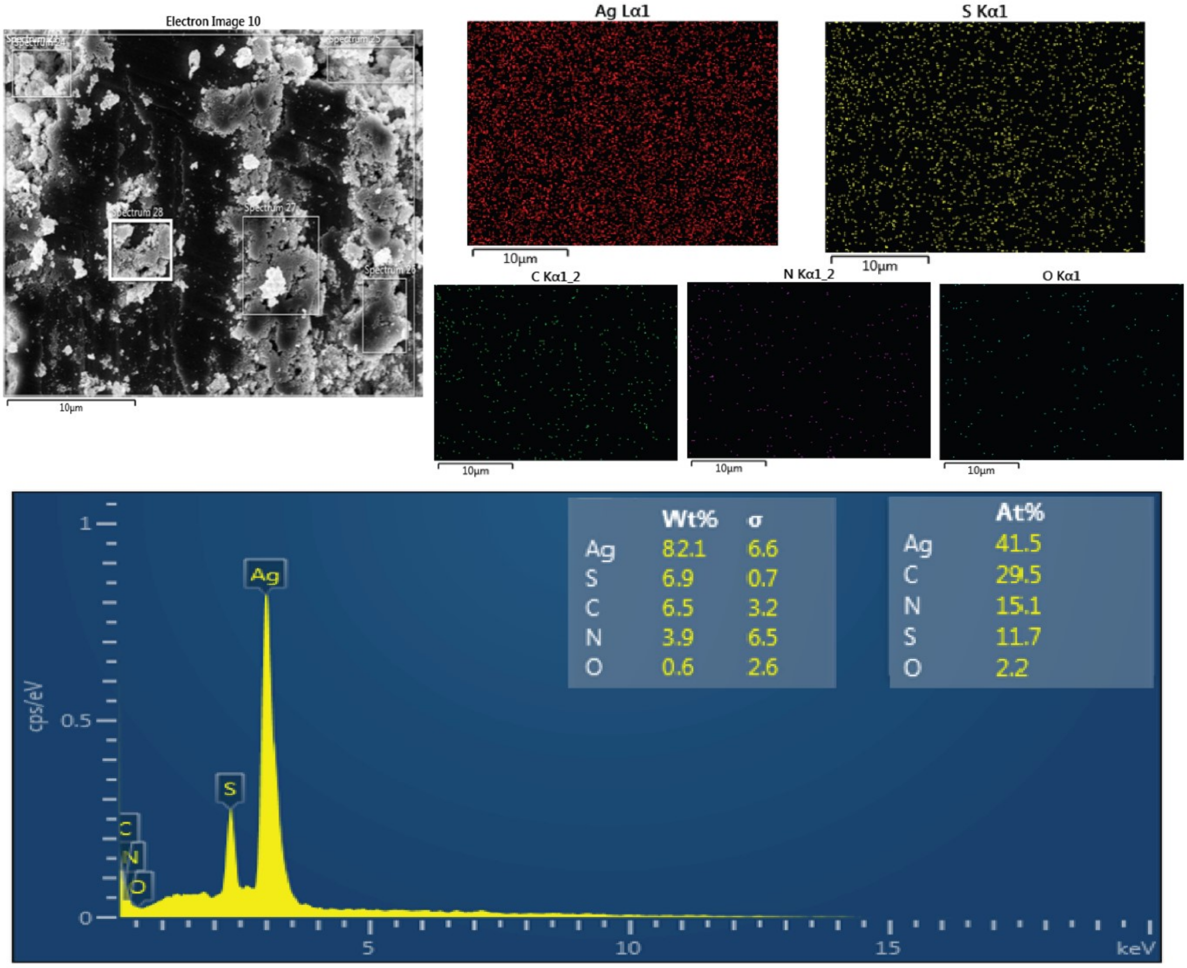

| | Wt% | σ |
|---|---|---|
| Ag | 82.1 | 6.6 |
| S | 6.9 | 0.7 |
| C | 6.5 | 3.2 |
| N | 3.9 | 6.5 |
| O | 0.6 | 2.6 |

| | At% |
|---|---|
| Ag | 41.5 |
| C | 29.5 |
| N | 15.1 |
| S | 11.7 |
| O | 2.2 |

**Figure S3. EDX analysis of T1 system.**

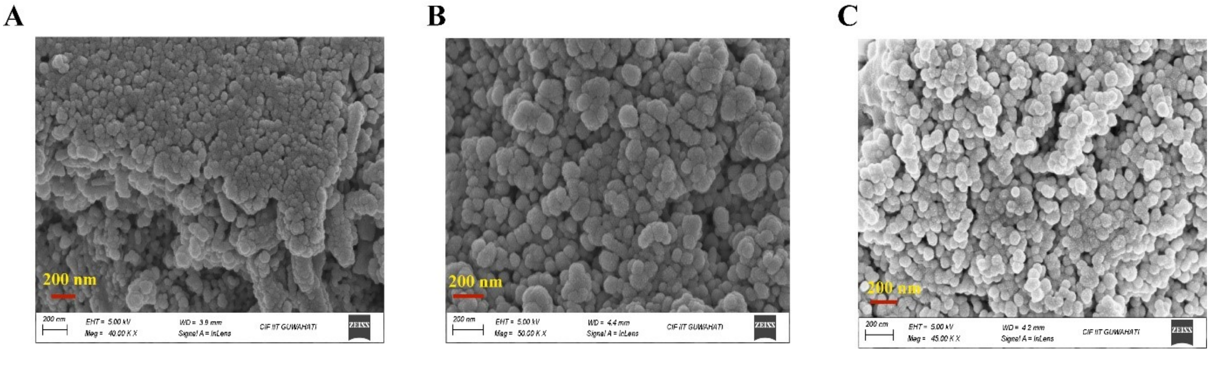

**Figure S4. SEM micrograph obtained for (A)T0 (B)T0.5 and (C)T1 systems.**

## TEM analysis

We have performed TEM characterisation of all the synthesised samples (T0, T0.5, and T1) (**Figure S5**). The T0, T0.5, and T1 possess the average particle size of 78, 40, and 32 nm, respectively. A similar decreasing trend is observed upon functionalisation like FESEM cluster sizes.

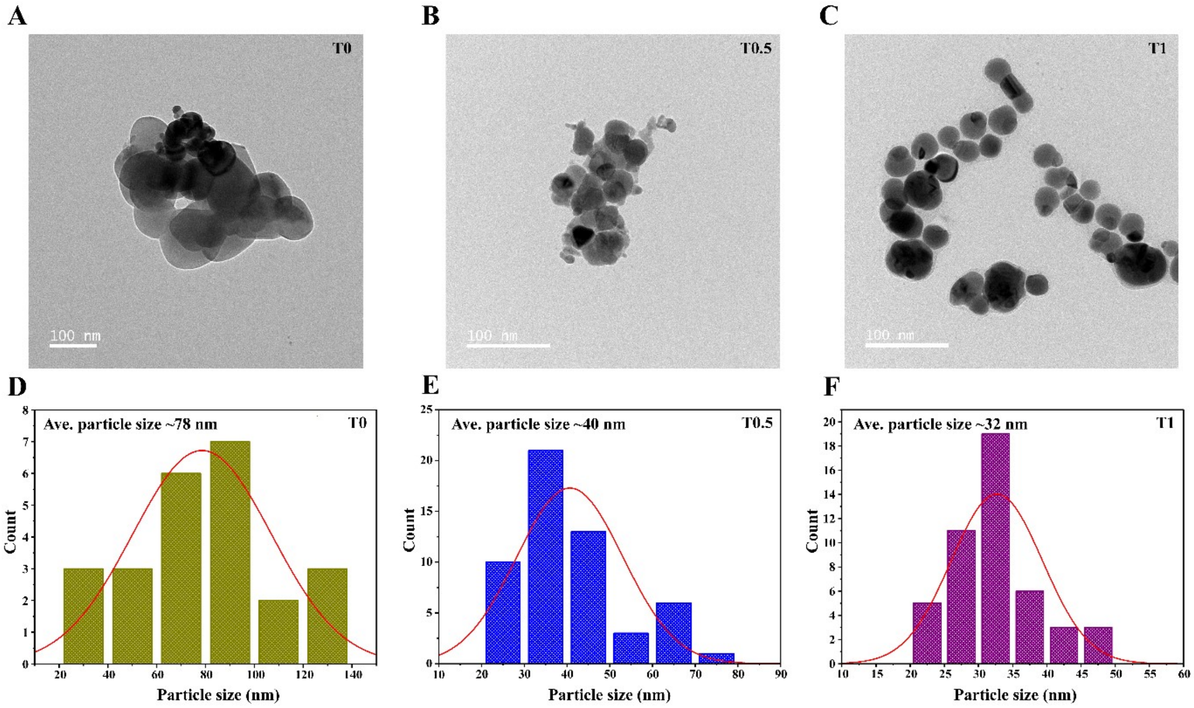

**Figure S5.** TEM images of (A) T0, (B) T0.5, (C) T1 and particle size distribution curve for (D) T0, (E) T0.5, (F) T1 samples

## Calculation details of molecular surface area:

Molecular surface area (MSA) computes the total exposed surface area of a molecule, from both polar and nonpolar atoms, and is critical to understand the molecular interactions and nanoparticle aggregation behaviour. In our study we have used maestro tool from Schrödinger suite to calculate MSA [1]. The detailed formula for calculating MSA involves estimating the solvent-accessible and van der Waals surface areas along with the sum of scaled hydrogen bond acceptor and donor surface areas, as follows:

$$S_{mol} = \sum_i \left( \frac{S_i}{S_{max,i}} \cdot A_i \right) + \sum_j \left( \frac{S_j}{S_{max,j}} \cdot B_j \right)$$

where $S_i$ and $S_j$ are the vdW or SASA areas for atoms i and j, $S_{max,i}$ and $S_{max,j}$ are the maximum exposed areas, and $A_i$ and $B_j$ are the hydrogen bond acceptor and donor strengths.

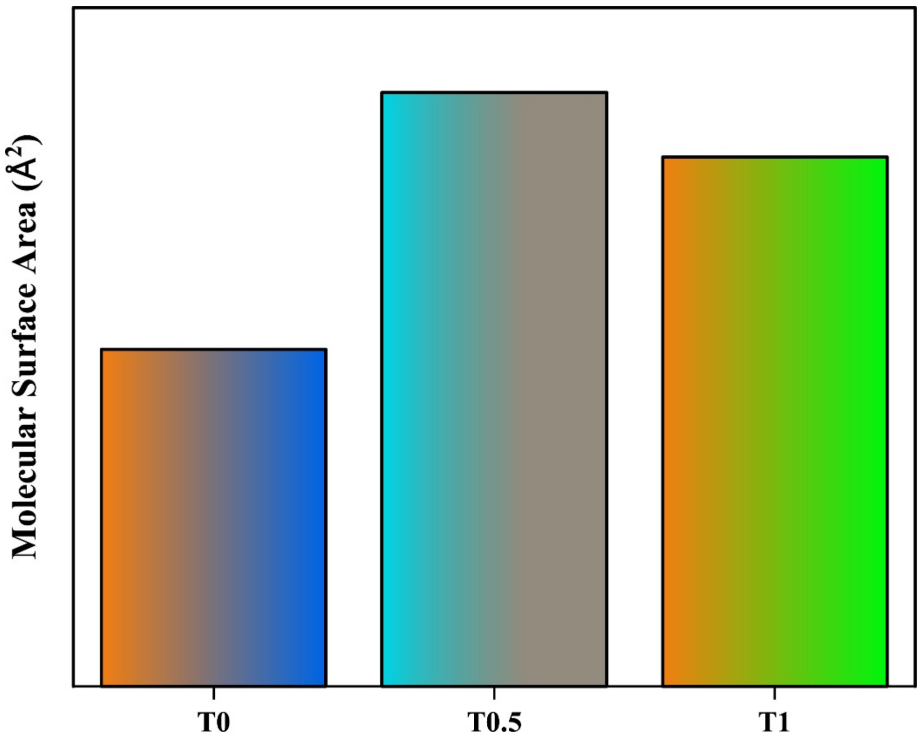

**Figure S6. Molecular surface area (MSA) of T0, T0.5, and T1 at 50 ns time scale.**

## Plasmonic stability

The absorbance data were collected in 10 minutes time intervals up to 1 hour. There is a negligible change in the plasmonic absorbance intensity as depicted in **Figure S7**. These results suggest a high plasmon stability in the functionalised system (T1).

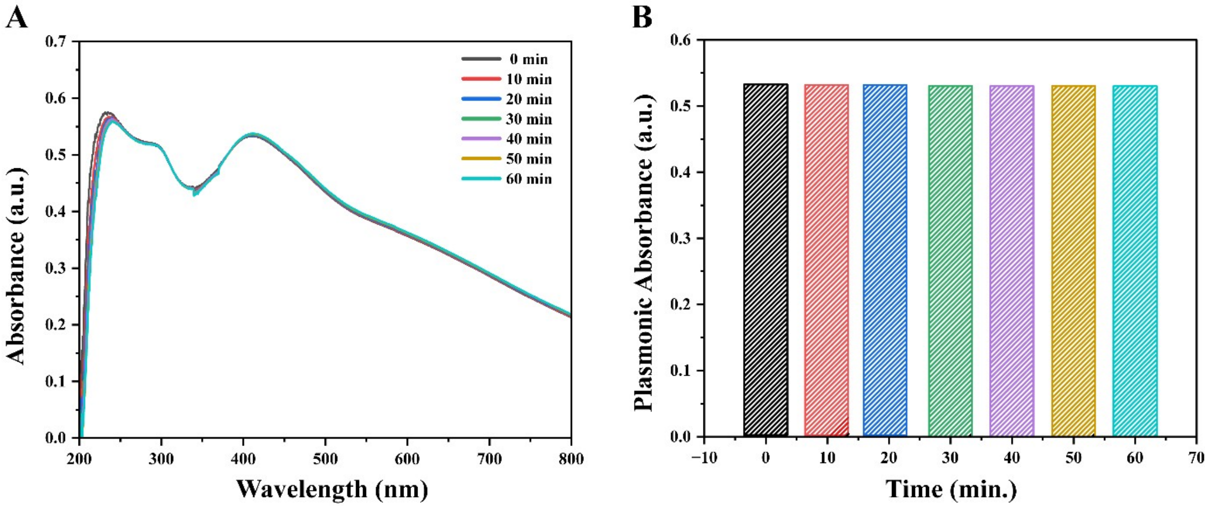

**Figure S7. (A) UV-Vis absorption spectra of T1 sample with different time intervals (B) Plasmonic absorbance intensities with different time intervals.**

## DFT mediated energetics analysis

The energy gap (ΔE) between the HOMO and LUMO orbital gives the system stability (**Table S4**). The highest gap in Ag-PVP indicates a slow electron transfer from HOMO to LUMO. It leads to less binding reactivity of the other molecules of interest on the cluster's surface. Tu decreases the ΔE introducing its atomic orbitals resulting in the reactivity. Additionally, the vacant and diffused d-orbitals could be effective in accommodating the extra electrons of adsorbates on the cluster's surface.

To compare oscillator strength (*f*) for Ag-PVP, Ag-PVP-Tu, and Ag-Tu, stick representations are depicted by incorporating three major non zero *f* values in Figure S5. The maximum *f* values are seen in Ag-Tu system, where lesser number of nonbonded electrons from hetero atoms are present. In the contrary, the minimum *f* values are detected for Ag-PVP-Tu system, where maximum number of nonbonded electrons are available. Thus, the incorporation of nonbonded electrons from PVP and Tu affects the overall electronic structure to influence the $n \rightarrow \pi^*$ transition represented as black line in Figure S5.

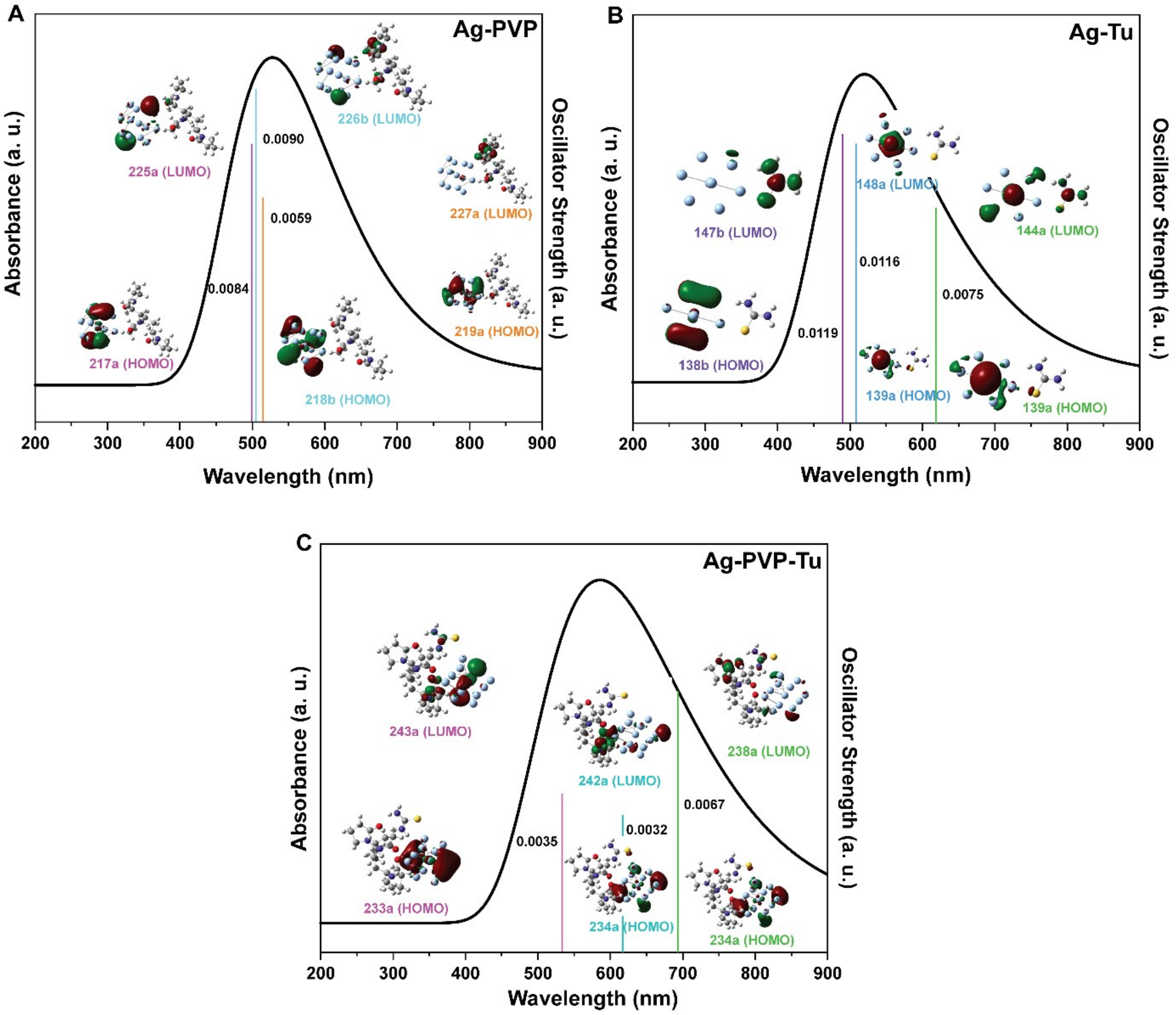

**Figure S8. Theoretical UV spectra (black) obtained with TD-DFT simulation of (A) Ag-PVP (B) Ag-Tu, and (C) Ag-PVP-Tu systems. The vertical excitation energies are shown in stick representation with number denoting the oscillatory strength.**

**Table S4. HOMO-LUMO energies of Ag-PVP, Ag-PVP-Tu, and Ag-Tu.**

| System | HOMO (α-state) (eV) | LUMO (α-state) (eV) | GAP (ΔE) (eV) |
|---|---|---|---|
| Ag-PVP | -3.51 | -2.18 | 1.33 |
| Ag-PVP-Tu | -3.18 | -2 | 1.18 |
| Ag-Tu | -4 | -2.76 | 1.24 |

## RDF analysis of T0.5 and T1 system

In this comparison RDF plot of Ag-$O^{PVP}$ for T0.5 and T1 systems a first coordination shell has been observed at ~1 Å for T1 system followed by many sharp subsequent peaks for both T0.5 and T1 system (**Figure S9**). These high number of peaks implies a greater number of distant coordination shell. This further reflects a well-defined coordination sphere of O around Ag atoms, which is clearly indicating the result from **Figure 2 (of main text)** that addition of Tu to the system gives the cluster a rigid and ordered structure.

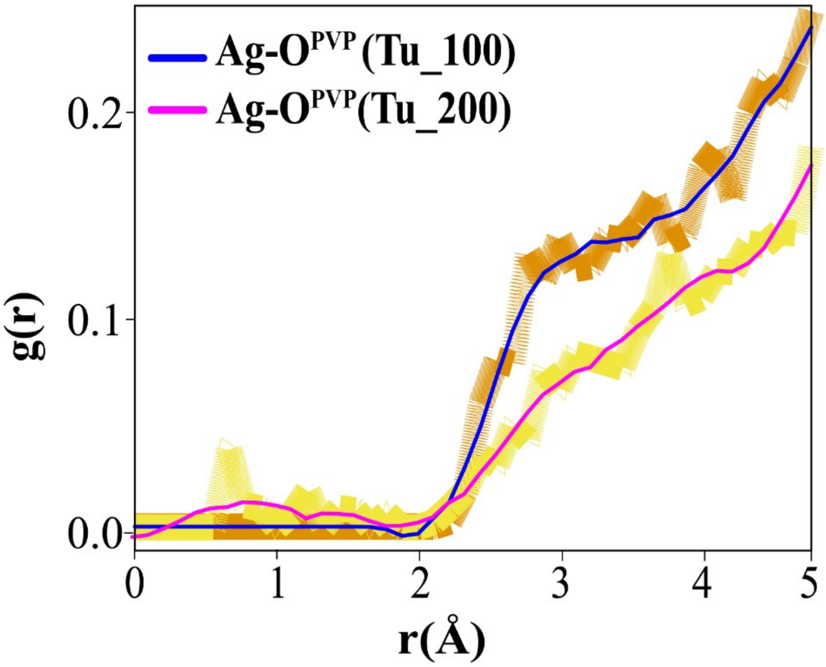

**Figure S9. Comparison of g(r) of $_{Ag-O}$$^{PVP}$ for T0.5 (Tu_100) and T1 (Tu_200) systems.**

## FTIR and XPS elemental analysis

**Table S5. XPS elemental composition of the T1 sample.**

| Region | Position | FWHM | Raw Area | %At Concentration |
|---|---|---|---|---|
| Ag 3d | 367.32 | 1.84 | 462021 | 55.70 |
| S 2p | 161.32 | 2.32 | 17909.6 | 23.23 |
| N 1s | 398.32 | 3.22 | 17435.1 | 21.07 |

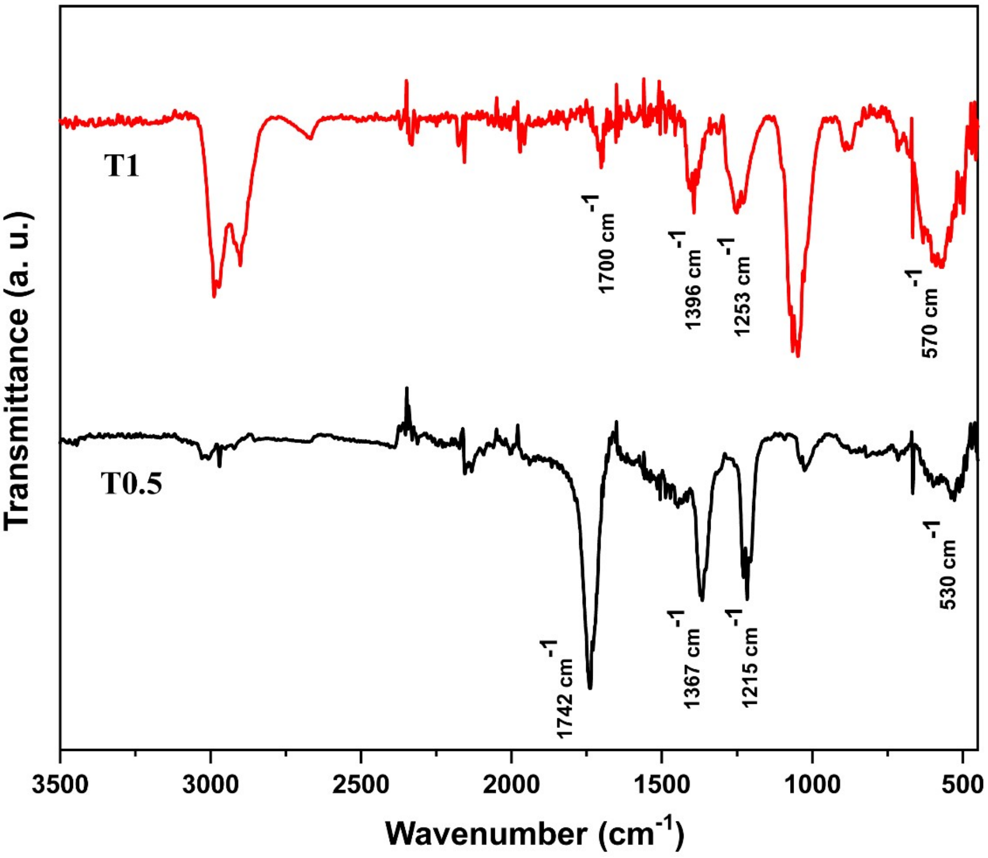

**Figure S10. FTIR spectra of T0.5 and T1 samples.**

## Binding energy and diffusion coefficient calculations

The binding interaction was studied through molecular docking through which we also calculated the binding energy. AutoDock 4.2.6 [2] with MGL Tools-1.5.7 [2] were used to perform blind molecular docking of PVP against Ag nanoclusters. This provides insights regarding the favorable binding site and helps in elucidating the binding energy of PVP while interacting with the Ag nanoclusters. Herein, we aim to compare the binding energy of PVP before and after sulfur functionalization. In the docking calculations, PVP is used as a ligand to dock over the Ag nanocluster. Gasteiger charges were assigned to PVP, and the structure was saved in the PDBQT format using MGL Tools-1.5.7. Ag nanoclusters were also preprocessed, parametrized and saved the structure in PDBQT format. The analysis of ligand protein interaction provides information about the intermolecular energies to determine the binding preference of PVP against Ag nanocluster.

The calculated binding energy of T1 (0.27 eV) is the highest, followed by T0.5 (0.25 eV) and T0 (0.22 eV) system. The observed trend in the binding energy explains the increased PVP binding affinity towards Ag nanoclusters after sulfur functionalization. Additionally, we also examined the role of PVP in stabilising AgNFs through mean square displacement (MSD) analysis. MSD is a fundamental tool for studying particle mobility and diffusion processes in molecular systems. The MSD is calculated as the average squared displacement of particles from their initial positions over time, through the equation below:

$$\mathrm{MSD}(t) = \langle |r(t+t_0) - r(t_0)|^2 \rangle$$

Where, $r(t)$ represents the position vector at time t; $t_0$ is the initial reference time; and ⟨⟩ denotes averaging over all particles and possible time origins

The MSD data plots were shown in **Figure S11**, which reveals that the activity of Ag nanoparticles is proportional to the slope of the MSD curve. The T1 system shows a distinctive diffusion pattern with very high initial mobility, reaching a peak around 600-700 $\text{Å}^2$. This rapid initial displacement indicates strong particle activity at the beginning of the simulation. However, the subsequent significant decrease in MSD values suggests that particles begin to form aggregates, restricting their mobility. A sublinear curve has been seen for T1 system having a peak around 600-700 $\text{Å}^2$, followed by a decline and secondary increase, suggesting sub-diffusion ($\mathrm{MSD} \propto t^{\alpha}$ where $\alpha<1$), often seen in crowded environments.[3] The sublinear curve of T1 system is due to the molecular crowding in the system as also discussed in section 4.2 of the main text. In T0.5 system, the most moderate diffusion pattern with a steady increase is revealed, reaching approximately 500 $\text{Å}^2$ in the last 10ns of simulation. The trend is consistently lowering in MSD trajectory, suggesting that the T0 system maintains a more compact structure throughout the simulation period. The T0 system demonstrates the highest displacement values, reaching approximately 900 $\text{Å}^2$ in the last 10ns. This continuous upward trend throughout the simulation indicates persistent dynamics with delayed aggregation compared to the T0.5 and T1 systems.

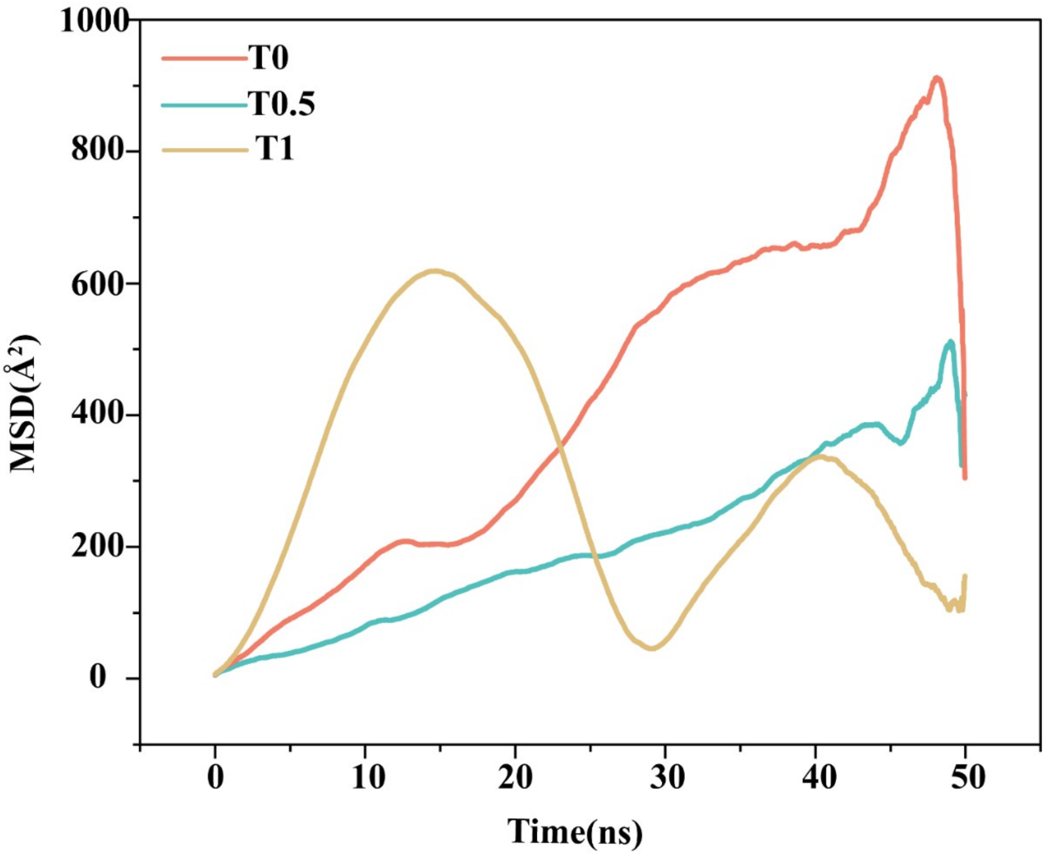

**Figure S11. MSD plots analysis of T0, T0.5, and T1 samples based on molecular dynamics simulations.**

Furthermore, to compare the diffusion behavior of Ag atoms after surface functionalization, mean square displacement (MSD) data has been calculated. The relationship between the MSD and diffusion coefficient can be expressed through an equation

$$\frac{1}{6}\lim_{t\to\infty}\frac{d}{dt}\langle\left|r(t+t^0)-r(t^0)\right|^2\rangle$$

Where, $r_i$ denotes the position vector of $i_{th}$ particle; and ⟨⟩ denote an ensemble average. The slope of the MSD curve as a function of time is proportional to the diffusion coefficient of the diffusing atoms. It is clear from the MSD data that T0 has the highest diffusion followed by T1 which shows sub-diffusion and T0.5 having moderate diffusion curve indicating the structural compactness. These observations suggest that the surface functionalization has caused a decrease in the diffusion of Ag atoms. This results in a steady diffusion behavior, indicating that the atoms are more likely to form clusters rather than moving freely.

## Surface energy calculations

The addition of sulfur to the system reduces the surface energy of the AgNFs, which promotes the formation of a more compact structure. The surface energy was calculated using the following formula, as implemented in a VMD Tcl script.[4]

$$\gamma = \frac{F_{\alpha\beta}}{A}$$

Where, $F_{\alpha\beta}$ is the free energy at the surface; A is the surface area; and $\gamma$ is the surface energy.

For the analysis of the surface energy, we considered the last 10 ns of the simulation trajectory. The overall results suggest sulfur functionalization leads to a significant reduction in surface energy. The T0 system exhibits the highest surface energy at 231.48 mJ/m². With the introduction of sulfur, the surface energy decreases to 155.31 mJ/m² for T0.5 and further to 170.42 mJ/m² for the T1 system. The slight higher surface energy for the T1 system in comparison to T0.5 is again due to the molecular crowding phenomenon as discussed in the above section. These results, shown in **Figure 12** indicate that increasing sulfur concentration lowers the surface energy, thereby favoring the formation of a denser and more compact AgNFs.

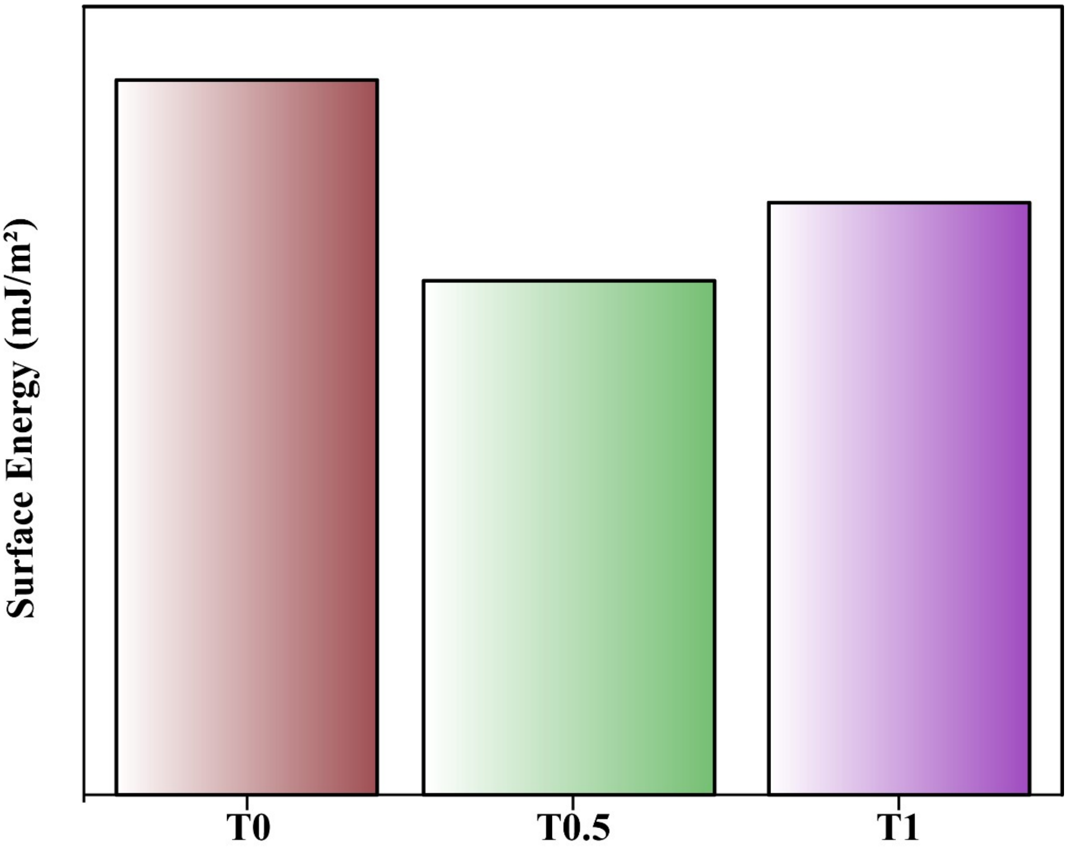

**Figure S12. Surface energy comparison of T0, T0.5, and T1 based on the last 10 ns of molecular dynamics simulation.**

## Radial Distribution Function analysis

The RDF or pair correlation function $g_{AB}(r)$ describes how particle density varies as a function of distance from a reference particle. It estimates the probability of finding a specific type of particle A at a distance r from a reference particle of type A, and is expressed with below equation [5]:

$$g_{AB}(r) = \frac{\langle \rho_B(r) \rangle}{\langle \rho_B \rangle_{local}} = \frac{1}{\langle \rho_B \rangle_{local}} \frac{1}{N_A} \sum_{i \in A}^{N_A} \sum_{j \in B}^{N_B} \frac{\delta(r_{ij} - r)}{4\pi r^2}$$

Where, $\langle \rho_B(r) \rangle$: Particle density of type $B$ at a distance $r$ around particles $A$; $\langle \rho_B \rangle_{local}$: Particle density of type $B$ averaged over all spheres around particles $A$ with radius $r_{max}$; $N_A$, $N_B$: number of particles of type A and B, respectively; and $r_{ij}$: distance between particle i∈A and j∈B

## Thermogravimetric analysis

Thermogravimetric analysis (TGA) experiment was performed to obtain the thermal behaviour of the functionalised system (T1), as shown in **Figure S13**. The weight loss occurs at three different regions, i.e. 112, 330, and 556 °C. The 6% total weight loss describes the high stability of the synthesised material.

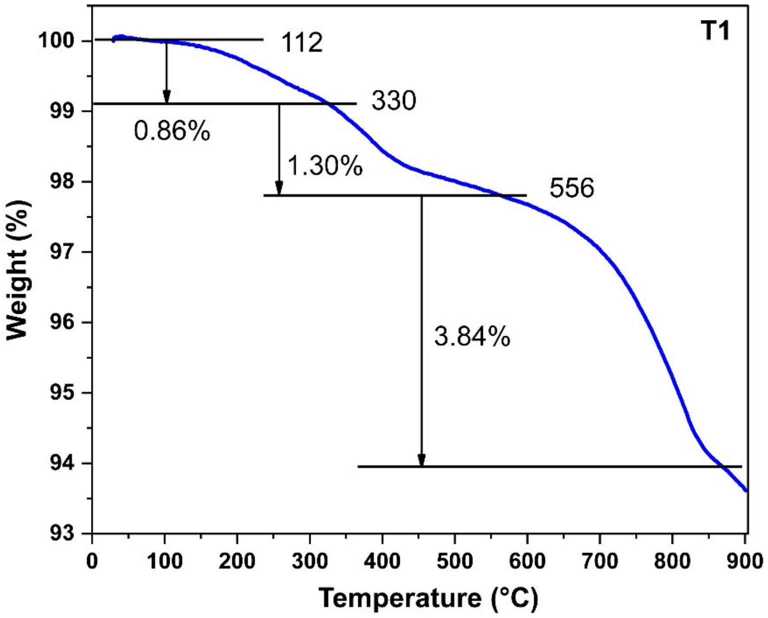

**Figure S13. TGA curve of T1 sample.**

## References

1 L. David, M. Wenlock, P. Barton and A. Ritzén, Prediction of Chameleonic Efficiency, *ChemMedChem*, 2021, **16**, 2669–2685.

2 G. M. Morris, H. Ruth, W. Lindstrom, M. F. Sanner, R. K. Belew, D. S. Goodsell and A. J. Olson, AutoDock4 and AutoDockTools4: Automated docking with selective receptor flexibility, *J Comput Chem*, 2009, **30**, 2785–2791.

3 M. B. Luo and D. Y. Hua, Simulation Study on the Mechanism of Intermediate Subdiffusion of Diffusive Particles in Crowded Systems, *ACS Omega*, 2023, **8**, 34188–34195.

4 R. Sedev, Surface tension, interfacial tension and contact angles of ionic liquids, *Curr Opin Colloid Interface Sci*, 2011, **16**, 310–316.

5 M. W. Terban and S. J. L. Billinge, Structural Analysis of Molecular Materials Using the Pair Distribution Function, *Chem Rev*, 2022, **122**, 1208–1272.